A RETROSPECTIVE SATELLITE ANALYSIS OF THE JUNE 2012 NORTH AMERICAN DERECHO

Kenneth Pryor

Center for Satellite Applications and Research (NOAA/NESDIS) College Park, MD

Belay Demoz

Physics Department, University of Maryland, Baltimore County

1. INTRODUCTION

Downbursts are strong downdrafts that induce an outburst of damaging winds at or near the ground, and a microburst as a very small downburst with an outflow diameter of less than 4 km and a lifetime of less than 5 minutes (Fujita 1985; Wakimoto 1985). The dangers posed by convective storm-generated downbursts have been extensively documented. Since 2000, the National Transportation Safety Board (NTSB) has recorded 48 downburst-related accidents over CONUS with 42 fatalities (National Transportation Safety Board 2021) that involved personal or instructional aircraft. Severe windstorms (i.e., widespread convective wind gusts > 25.7 m s−1 (50 kt)) resulting from mesoscale convective systems (MCS) cause significant disruption to society, including widespread power outages, tree and structural damage, and transportation accidents that affect multi-state regions and metropolitan areas along their track. Among them, a derecho, defined as a long-lived, widespread severe convective windstorm, is composed of numerous downbursts that are organized into clusters or families of clusters. Derechos can produce winds above hurricane force along a track that may exceed several hundred kilometers. Between 1987 and 2002, severe convective windstorms resulted in a total property loss of over $3 billion in the United States, with an average loss per event of $96 million. Also, between 1986 and 2003, severe convective windstorms were responsible for a total of 153 deaths and 2605 injuries, proving to be more deadly and hazardous than the low-end (F-0/F-1 intensity) tornado outbreaks that occurred during the same period and resulted in only 71 deaths (Ashley and Mote 2005). Because these

events are severe, it is important to understand the factors that lead to the downbursts and utilize all available observations to monitor and forecast their development.

Convective windstorm potential has been traditionally expressed as a grouping of stability parameters relevant for downburst generation. These include the lower-to-mid-tropospheric temperature and equivalent potential temperature (theta-e) lapse rates, vertical relative humidity differences, and the amount of convective available potential energy (CAPE) in the troposphere. Some factors increase the likelihood of severe convective winds, which are (1) an elevated mixed layer that promotes instability by generating powerful storm updrafts and downdrafts (Banacos and Ekster 2010) and (2) a rear-inflow jet into an MCS (Smull and Houze 1987; Weisman 1992) which channels unsaturated mid-tropospheric air into the leading convective storm line. The establishment of an elevated, ascending front-to-rear flow originating from deep, moist convection, overlying a strong and deep outflow-induced cold pool has been found to generate and sustain a robust rear inflow jet (Weisman 1992). Other factors can reduce the likelihood of severe convective winds, such as the presence of a lower-tropospheric temperature inversion and a surface-based layer of unsaturated air that reduces virtual temperature.

During the morning of 29 June 2012, an area of multicell convective storms developed over Iowa and then organized into a quasi-linear convective system (QLCS) as it tracked into northern Illinois. The system then evolved into a bow echo (Przybylinski 1995) during the afternoon and tracked rapidly southeastward over the Ohio Valley to the Mid-Atlantic coast by late evening. What would eventually become the 29 June 2012 North American Derecho, this QLCS produced its first significant severe downburst, with winds measured over 65 knots, at Michigan City, Indiana during the early afternoon. This extraordinary derecho-producing convective system (DCS) event resulted in 22 deaths and nearly a thousand severe wind reports

from northern Illinois to the Atlantic Coast. This system was more typical of a warm-season progressive derecho, associated with a major heat wave and an elevated mixed layer (Banacos and Ekster (2010)). This DCS was generated and then propagated within a mid-tropospheric ridge synoptic pattern as identified by Johns (1993) and Coniglio et al. (2004). During the evening of 29 June, the derecho tracked rapidly eastward across the mountains of West Virginia (WV), western Virginia (VA), southwest Pennsylvania (PA), and western Maryland (MD) during mid-evening. The derecho's effects were particularly formidable in the Washington, DC – Baltimore, MD corridor, where measured wind gusts of 60-70 knots severed numerous overhead electrical feeders.

This paper presents a discussion of the science of operational forecasting of severe windstorms through examples of employing new satellite and ground-based microwave and vertical wind profile data. Accordingly, this paper is organized as follows: Section 2 is a detailed background of severe convective windstorm theory that includes a discussion of windstorm genesis and evolution. Section 3 is a summary of instrumentation and measurement application methodology. Finally, as an example of the coordinated use of surface- and satellite-based observational instrumentation, section 4 presents a discussion of the evolution and intensification of the DCS over the U.S. Appalachian Mountain and Mid-Atlantic coastal regions.

2. BACKGROUND AND THEORETICAL CONSIDERATIONS

The outline of convective windstorm theory begins with the requirement that severe storms are highly organized. Downdraft initiation proceeds as a departure from hydrostatic equilibrium. For a volume of air with a high concentration of ice phase precipitation that develops within a convective storm, the resultant force F on the precipitation volume is downward and imparts negative buoyancy. This physical basis can be extended to more complex convective systems in which updrafts, downdrafts, and outflow foster a rear inflow jet’s development.

2.1 *Storm Microphysical and Thermodynamic Processes*

The standard NOAA/National Weather Service (NWS) definition of a severe thunderstorm includes damaging winds with gusts of 26 m s-1 (50 kt) or greater and hail with a diameter of 2.5 cm (1 inch) or greater. Severe thunderstorms are most identifiable in weather radar imagery, in which a large concentration of ice-phase precipitation within a volume results in high reflectivity resulting from increased backscattering. Downdraft severity is governed by phase change and the loading of ice-phase precipitation. Loading, in effect, refers to the mass of a collection of hydrometeors. When gravity is imposed upon the volume of hydrometeors, downward acceleration occurs due to precipitation's weight.

A prototypical conceptual model of a deep moist convective (DMC) storm is shown in Figure 1a. Srivastava (1987) found that precipitation in the form of ice increases the convective downdraft intensity. This effect increases with precipitation content and the stability of the environmental lapse rate of temperature. The power of the downdraft also increases in proportion to the relative concentration of smaller particles. Condensate loading (Srivastava 1987), sometimes combined with subsaturated air entrainment in the storm middle level (Knupp 1989), initiates the convective downdraft. The subsequent melting of frozen hydrometeors and subcloud evaporation of liquid precipitation, in conjunction with precipitation loading, result in the cooling and negative buoyancy that accelerate the downdraft in the unsaturated layer (Srivastava 1987). The melting of ice-phase precipitation, subsequent evaporative cooling, and the resulting downdraft strength are enhanced by sizeable liquid water content and the related water surface available for evaporation. A large lapse rate maintains negative buoyancy as the downdraft descends in the subcloud layer (Srivastava 1987). As the lapse rate's stability is increased, higher precipitation contents, precipitation in the form of ice, and relatively higher concentrations of small precipitation particles

are required to force an intense downdraft. At this point in the downdraft initiation process, potential energy resulting from temperature deficit between the precipitation-infused parcel and the ambient environment is converted to downward air parcel motion, which, collectively, comprises the convective downdraft. As the lapse rate becomes even more stable, only wet downbursts having substantial precipitation in the form of ice are possible. A downburst can be driven solely below the cloud base where melting and evaporation of precipitation and precipitation loading below the cloud base were sufficient to produce wet downbursts.

Knupp (1989, 1996) refined the understanding of the downburst generation's physical and dynamic processes. The author noted that low-level downdrafts are closely controlled by the arrival of precipitation at low levels. In the storm middle levels, air flows quasi-horizontally around the updraft flanks and converges into the downshear flank, referred to as the wake. Within the wake region, where entrainment reduces positive buoyancy and associated updraft strength, precipitation at middle levels (where it is grown most effectively) is then allowed to descend to lower levels. The intrusion of drier air into the wake's precipitation region also enhances the evaporation/sublimation process. Diabatic cooling from melting and evaporation is most effective at levels below the melting level. Convergence within the downshear wake is thus instrumental in transporting precipitation into the downshear flank. Therefore, a comprehensive understanding of the downdraft initiation process is closely related to the precipitation initiation and transport process within clouds and is observable in passive MW imagery, as shown in this study. Such processes depend not only on vertical profiles of temperature and moisture but also on vertical environmental wind profiles. Knupp (1996) identified the protrusion echo produced by settling hydrometeors from a line of weak updraft that formed in association with low-level confluence located east of the storm core. The protrusion appeared to be partly forced by existing mesoscale

convergence, while the updraft within its lower levels represented the weak low-level ascent along the up-down downdraft branch. In this regard, the protrusion was indirectly connected to the strong core downdraft. Initial bowing of the echo (Przybylinski 1995) was associated with the early microburst activity, a characteristic observed in other case studies. The inference of downburst occurrence can be successfully applied by the synergistic use of satellite-based passive MW and ground-based Doppler radar data and imagery.

2.2 ***Storm Dynamic Processes***

From Weisman, Klemp, and Rotunno (1988) as a departure point, Weisman (1992) explored the role of vertical wind shear and buoyancy in the generation of a rear inflow jet and visualized the associated conceptual model of this process. Weisman (1992) noted that rear inflow is generated in response to the development of an upshear-tilted updraft, as the horizontal buoyancy gradients along the back edge of the expanding system create a circulation that draws midlevel air in from the rear. The rear inflow jet system can take two forms, descending and elevated. For a descending-jet system, the convective circulation is characterized by an updraft current that ascends gradually above a spreading surface cold pool, with light-to-moderate convective and stratiform rainfall extending well behind the leading edge of the cold pool. This structure is often associated with a decaying system. The gust-front lifting is not strong or deep enough to regenerate new convective cells, and the mesoscale circulation slowly weakens. However, for an elevated-jet system, the circulation is dominated by strong, erect updrafts along the leading edge of the surface cold pool, with the updraft current spreading rapidly rearward above 7-8 km above ground level. Moderate-to-heavy convective rainfall exists at the system's leading edge, with lighter rainfall extending to the rear. This structure tends to be longer-lived than the descending-jet case, as the deeper gust-front lifting regularly regenerates strong convective cells.

The rear-inflow jet represented a new, potentially significant horizontal vorticity source that must be included when diagnosing various circulation sources' relative importance. Specifically, a rear-inflow jet that descends and spreads along the surface is characterized by the same sign of horizontal vorticity generated by the cold pool, thereby accentuating the cold pool circulation.

In contrast to a descending jet, an elevated rear-inflow jet is characterized by the opposite sign of horizontal vorticity generated by the cold pool (up to jet level), thereby accentuating the ambient vertical shear effects. Since significant rear-inflow characteristically develops after the cold-pool circulation overwhelms the ambient shear, a surface jet's development reinforces the upshear-tilting process that tends to weaken the system. However, an elevated rear-inflow jet's development reverses this process, promoting powerful, upright convective cells along the cold pool's leading edge. Johns (1993) built on the basis established by previous observational and modeling studies of environmental conditions associated with the development and maintenance of bow echo-induced damaging winds, focused on parameters related to storm outflow and updraft strengths. Specifically, wind speeds and relative humidity values in the mid-levels (related to outflow strength) and instability (related to updraft strength) were examined. The results indicated that these parameters exhibit a wide range of values when considering all bow echo situations in which damaging winds are reported. Further, combinations of wind speeds in the mid-levels and instability tend to vary with the season and the synoptic situation. For example, when powerful winds are present in the mid-levels, bow echo development has been observed in only marginally unstable environments. Bow echo events associated with the powerful wind-marginal instability combination typically occur with strong, rapidly moving low-pressure systems ("dynamic" synoptic pattern) in the colder months of the year. On the other hand, events associated with the relatively weak wind-extreme instability combination typically occur along a quasi-stationary

thermal boundary in relatively stagnant weather regimes ("warm season" synoptic pattern) in the late spring or summer. Many bow echo wind events are associated with wind-instability combinations between the extremes. Some of these events are related to synoptic patterns that do not sufficiently match either prototypical pattern.

3. METHODOLOGY

Surface-based measurements in the radio and microwave regions of the electromagnetic spectrum provide important environmental parameters for monitoring atmospheric stability and mesoscale and microphysical processes associated with convective storm development. Over CONUS, traditional datasets applied to both operational downburst monitoring and prediction, as well as product validation, include surface-based observations of atmospheric parameters (i.e., temperature, humidity, wind speed/direction, sky condition, precipitation accumulation, etc.) from NWS/FAA aviation routine meteorological reports (METAR) stations, mesonetwork (mesonet) stations, radiosonde observations, and meteorological Doppler radar reflectivity and velocity measurements. In effect, surface weather observation and analysis represent a primary important step in convective storm diagnosis process.

An ultra-high frequency (UHF) Boundary Layer Profiler (BLP) is capable of identifying mesoscale features such as low-level jets, rear-inflow jets, and convective storm outflow and can supplement the Next Generation Weather Radar (NEXRAD) velocity azimuth display wind profile (VWP) product at longer distances (> 30 km) from the adjacent NEXRAD site. The BLP is a Doppler radar system operating at a frequency of 915 MHz that provides high-resolution observations with enhanced sensitivity to hydrometeors (Eklund et al. 1987) in which backscattered signals from turbulence-induced refractive index variations are detected by the radar (Martner et al. 1993). The BLP retrieves horizontal wind speed and direction up to an elevation of

four kilometers above ground level at a vertical resolution of 60 m. In selected regions of CONUS, an expanded dataset incorporates lower tropospheric vertical wind profile data. The BLP at Howard University Beltsville Campus (HUBC), near Washington DC, was in operation during the derecho passage and provided near real-time wind observations. The HUBC BLP provides the most representative wind conditions in the Washington, DC metropolitan area. These BLPs are component of the Cooperative Agency Profilers (CAP) network, which compiles data in real-time, applies quality control, and distributes the data online. Current and archived BLP wind data is available on the CAP website: https://madis-data.ncep.noaa.gov/cap/

In addition, as noted in Figure 2, vertical temperature and moisture sounding datasets generated by the surface-based microwave radiometer profiler (MWRP) provide routine monitoring of thermodynamic patterns in both the pre-convective and storm environments (Westwater et al. 2005). In the Washington, DC – Baltimore, Maryland corridor, MWRPs at Germantown, Maryland and HUBC, manufactured by Radiometrics Corporation, observes atmospheric brightness temperatures in 12 frequency bands from 22 to 59 GHz and retrieves temperature and humidity soundings up to 10 km height with a vertical resolution of 50 m below 500 m AGL and a resolution of 100 m between 500 and 2000 m AGL. The MWRP exploits the 30 to 50 GHz transmission window to retrieve water vapor profiles, while exploiting the absorption band near 60 GHz for temperature sensing. The HUBC MWRP employs the neural network (NN) inversion method of retrieval, trained with a large dataset of profiles generated from historical datasets of operational radiosondes. Vertical temperature and humidity profiles are often applied to calculate CAPE. This paper demonstrates the thunderstorm downburst potential applications of the microburst windspeed potential index (MWPI, Pryor 2015) as calculated from MWRP and satellite sounding datasets.

As outlined in Figure 2 and shown in Figures 3 and 4, the June 2012 North American Derecho was observed simultaneously by the microwave sensors onboard polar-orbiting meteorological satellites, vertical sounding profiles generated from the Infrared Atmospheric Sounding Interferometer (IASI), NEXRAD systems, and MWRPs. Data collection, processing, and visualization follow the methodology of Pryor (2015, 2017). We use microwave sensors on the Meteorological Operational (METOP)-A satellite where Microwave Humidity Sounder (MHS) 89 GHz window channel datasets were obtained from the NOAA Comprehensive Large Array-data Stewardship System (CLASS) and the EUMETSAT Data Centre. Vertical temperature and wind profile data, up to 5 km above ground level, from the CAP network are applied to further study the favorable environment for severe convective storm winds.

The Next Generation Weather Radar (NEXRAD) level-II reflectivity and radial velocity are obtained from the National Center for Environmental Information (NCEI) and used to verify that observed wind gusts are associated with downbursts originating from high reflectivity factor storms and are not associated with other types of convective wind phenomena (i.e., gust fronts). Plan-view images of radar reflectivity are constructed from the lowest elevation angle scan (0.46°). An additional application of radar reflectivity factor imagery is to infer microscale physical properties of downburst-producing convective storms. Particular reflectivity signatures, such as bow echoes (Przybylinski 1995) and protrusion echoes (Knupp 1996), are effective indicators of downburst occurrence. Downburst occurrence can be further confirmed by calculating a surface ΔT value, where $\Delta T \equiv T(\text{downburst}) - T(\text{ambient})$ and represents the peak temperature departure from ambient at ground level (Proctor 1989). ΔT can therefore serve as a proxy variable for the surface density perturbation through the ideal gas law. In summary, a comprehensive approach of observational data analysis involves both surface- and satellite-based instrumentation. Because

this approach utilizes operational products available to weather service forecasters, it can feasibly be used for monitoring and forecasting downburst occurrence. Compared to other ground-based microwave imagery sources, such as Doppler radar, spatial patterns in TB can also infer airflow characteristics and circulation patterns surrounding the convective storm of interest.

4. DISCUSSION: DCS EVOLUTION AND IMPACT

As the derecho system tracked from the Ohio Valley through the Appalachian Mountain region, the spatial structure transitioned from a large bow echo to a quasi-linear convective system (QLCS) with a protrusion consisting of a cluster of high-reflectivity storms at the northern terminus of the line, as shown in Figure 3. Interestingly, the increase in radial velocity as measured by the Sterling, Virginia NEXRAD (LWX) near 0200 UTC 30 June, apparent in Figure 4, signified in strengthening of the rear-inflow jet (RIJ) feeding the rear flank of the DCS. Comparison of the late evening METOP-A Infrared Atmospheric Sounding Interferometer (IASI) sounding near Salisbury, Maryland to the Germantown and HUBC microwave radiometer sounding profiles at 0200 UTC 30 June in Figures 5, 6, and 7, exhibits a transition to a moist and highly unstable profile favorable for severe wet microbursts. Figure 5 illustrates the sounding modification process to further enhance the signal for severe deep convective storm development. In Figure 5a, the IASI thermodynamic profile indicated modest convective storm potential. Incorporating the 0154 UTC surface temperature and dew point observation from Salisbury Regional Airport (27 km (14 n mi) north of the IASI retrieval site), as shown in Figure 5b, results in significantly larger CAPE. Finally, substituting the dry bulb temperature dataset with calculated virtual temperature yields the strongest signal for severe downburst generation with wind gust potential of 57 knots, comparable to the potential derived from the Germantown and HUBC MWR soundings as demonstrated in Figures 5c, 6 and 7. Accordingly, the MWPI increased in magnitude prior to the onset of the

derecho to eventually indicate convective wind gust potential of 55-59 knots with an hour of lead time. Between 0000 and 0200 UTC, as shown in Figure 8, the DCS evolved into a double-bow echo pattern with a "warm advection wing" (Smith 1990) over Frederick County (near latitude 39.5°N/longitude 77.4°W) that developed in an east-west oriented region of weak surface convergence over central Maryland.

Figure 8 exhibits a type 2 derecho echo pattern with a warm advection wing (Przybylinski 1995) that extended downwind (eastward) from the northern end of the bulging line echo. Microbursts occurred in Frederick County, Maryland within the warm advection wing of the derecho. METOP-A MHS, with overlying Sterling, VA (LWX) NEXRAD reflectivity, revealed the presence of the warm advection wing. A dry air notch, displayed as an inward (eastward) pointing TB gradient, likely indicated the presence of a rear-inflow jet ("RIJ") that sustained the MCS and the generation of downburst clusters in the DC-Baltimore corridor during the following hour. Subsequent new bow echo development over Maryland, northwest of Washington, DC, after 0200 UTC is well apparent in Figure 9. Close-up Sterling NEXRAD Constant Altitude – Plan Position Indicator (CAPPI) images at 0.3 and 2.5 km altitude, respectively, show high reflectivity values extending upward into the mid-levels of the leading convective storm line while moving over the Germantown MWRP. Consequently, a time-height cross-section of equivalent potential temperature (θ_e) deviation ($\theta_e - \theta_{e\,mean}$) between 0144 UTC and 0244 UTC that tracked the passage of the leading convective storm line, indicated elevated values associated with strong microwave thermal emission of melting graupel and hail (between 0230 and 0250 UTC). The presence of relatively dry (low θ_e) mid-tropospheric air prior to the onset of the leading storm line (i.e., downwind of the DCS) and possibly entrained into the precipitation core, was represented by large negative θ_e deviation (< -20 K). An important subsequent exercise entailed comparison of MWRP

physical parameters to LWX high resolution digital vertically integrated liquid (DVIL) as demonstrated in Figure 10. Figure 10a shows a close correspondence between MWRP liquid density and NEXRAD DVIL while Figure 10b shows a similar relationship between MWRP-derived θ_e and DVIL. Interestingly, a mid-tropospheric θ_e minimum after the passage of the leading convective storm line was coincident with low liquid density (g m^{-3}) and correspondingly low values of DVIL from 0250 to 0350 UTC. This relationship between the liquid, DVIL, and θ_e parameters likely signifies the passage of the DCS trailing stratiform precipitation region, typically found in close proximity to the RIJ. As shown in Figures 11 and 12, the RIJ was apparent and distinguishable from surface-based outflow in the Sterling, Virginia NEXRAD VWP and Beltsville, Maryland 915 MHz Boundary Layer Profiler (BLP) wind observation time series, respectively. The sustained elevation of the lower-to-middle tropospheric wind maximum after the passage of the leading convective storm line suggests the occurrence of an elevated RIJ. The combination of the presence of a trailing stratiform precipitation region and corresponding mid-tropospheric θ_e minimum as shown in Figure 10 affirms the development of an RIJ as described in section 2.2. One of the first severe wind reports in the Washington, DC metropolitan area was 62 knots recorded at 0228 UTC at Dulles International Airport. Near 0250 UTC, a downburst cluster tracking over downtown Washington, DC produced measured wind gusts of 61 and 47 knots at Reagan National Airport and the Washington Physical Oceanographic Real-Time System (PORTS) station, respectively. A gust factor (Choi and Hidayat 2002) of 1.42 and ΔT values of -10 to -11°C were also consistent with downburst occurrence embedded in the larger-scale DCS.

5. CONCLUSIONS

In retrospect, NWS/Storm Prediction Center (SPC) adequately indicated the likelihood of scattered severe winds over the Washington, DC – Baltimore, MD corridor as the derecho tracked east of

the Appalachian Mountains during the late evening. However, the density and magnitude of severe wind events, and associated impacts, over the Washington, DC metropolitan area, including the adjacent Maryland and Virginia suburbs, was not anticipated by neither SPC nor the NWS Office Baltimore-Washington. Thus, science value added with this case study entails the application of evening IASI/NUCAPS sounding profiles and derived parameters that will provide more insight to the evolution of the nocturnal convective lower troposphere. MW window channel data will more effectively interrogate evolving DCSs and reveal greater detail of storm structure, especially pertaining to convective wind generation.

Convective storm-generated downbursts are an operational forecasting challenge due to the spectrum of time, space, and intensity scales in which they occur. This paper assembled the governing physical theory essential for development of downburst prediction algorithms that proceeds from vertical momentum equations and the aggregate of thermodynamical and microphysical processes of precipitation. Accordingly, downburst monitoring and subsequent prediction is a three-step process with an objective to build a three-dimensional model of the thermodynamic structure of the ambient environment and conceptual model of downburst-producing convective storms:

1. Collection and exploitation of surface-based observations including measurements from tower platforms and Doppler radar-measured reflectivity and wind velocity.
2. Ground-based microwave and radio profiler instruments, including MWRPs and BLPs, to obtain vertical profiles of temperature, humidity, and wind velocity.
3. Satellite-based 2-D plan view images of brightness temperature and vertical profiles of temperature and humidity. Modification of sounding profiles with surface observations of

temperature and humidity is an additional step that results in improved representation of the ambient environment.

The study of the June 2012 Derecho demonstrates how both ground-based and satellite-based observational data for convective storms can be combined for monitoring and forecasting applications. Field measurements are the cornerstone for remote sensing techniques and are essential for understanding deep convective storms and associated downburst occurrence, phenomena that encompass the vertical dimension of the troposphere.

6. REFERENCES

Ashley, W. S., and T. L. Mote, 2005: Derecho Hazards in the United States. Bull. Amer. Meteor. Soc., 86, 1577–1592.

Atkins, N. T., and R. M. Wakimoto, 1991: Wet microburst activity over the southeastern United States: Implications for forecasting. Wea. Forecasting, 6, 470–482.

August, T., Klaes, D., Schlüssel, P., Hultberg, T., Crapeau, M., Arriaga, A., O'Carroll, A., Coppens, D., Munro, R. and Calbet, X., 2012. IASI on Metop-A: Operational Level 2 retrievals after five years in orbit. Journal of Quantitative Spectroscopy and Radiative Transfer, 113(11), pp.1340-1371.

Banacos, P.C., and M.L. Ekster, 2010: The association of the elevated mixed layer with significant severe weather events in the Northeastern United States. Wea. Forecasting, 25, 1082-1102.

Bloch, C.; Knuteson, R.O.; Gambacorta, A.; Nalli, N.R.; Gartzke, J.; Zhou, L. Near-Real-Time Surface-Based CAPE from Merged Hyperspectral IR Satellite Sounder and Surface Meteorological Station Data. J. Appl. Meteor. Clim. 2019, 58, 1613–1632.

Brock, F. V., K.C.Crawford, R. L. Elliott, G.W. Cuperus, S. J. Stadler, H. L. Johnson, and M. D. Eilts, 1995: The Oklahoma Mesonet: A technical overview. J. Atmos. Oceanic Technol., 12, 5–19.

Choi, E. C., and F.A. Hidayat, 2002: Gust factors for thunderstorm and non-thunderstorm winds. Journal of wind engineering and industrial aerodynamics, 90(12-15), 1683-1696.

Cimini, D., M. Nelson, J. Güldner, and R. Ware, 2015: Forecast indices from a ground-based microwave radiometer for operational meteorology. Atmospheric Measurement Techniques, 8(1), 315-333.

Coniglio, M. C., D. J. Stensrud, and M. B. Richman, 2004: An observational study of derecho-producing convective systems. Wea. Forecasting, 19, 320-337.

Ecklund, W. L., D.A. Carter, and B.B. Balsley, 1988: A UHF wind profiler for the boundary layer: Brief description and initial results. Journal of Atmospheric and Oceanic Technology, 5(3), 432-441.

Ellrod,G. P., 1989: Environmental conditions associated with the Dallas microburst storm determined from satellite soundings. Wea. Forecasting, 4, 469–484.

Esmaili, R.B.; Smith, N.; Berndt, E.B.; Dostalek, J.F.; Kahn, B.H.; White, K.; Barnet, C.D.; Sjoberg, W.; Goldberg, M. Adapting Satellite Soundings for Operational Forecasting within the Hazardous Weather Testbed. Remote Sens. 2020, 12, 886. https://doi.org/10.3390/rs12050886

Ferraro, R.R., Kusselson, S.J. and Colton, M., 1998: An introduction to passive microwave remote sensing and its applications to meteorological analysis and forecasting. National Weather Digest, 22, 11-23.

Ferraro, R., Beauchamp, J., Cecil, D., and Heymsfield, G., 2015: A prototype hail detection algorithm and hail climatology developed with the Advanced Microwave Sounding Unit (AMSU). Atmospheric Research, 163, 24-35.

Fujita, T. T., 1985: The downburst, microburst and macroburst. Satellite and Mesometeorology Research Paper 210, University of Chicago, 122 pp.

Fujita, T. T., and R. M. Wakimoto, 1981: Five scales of airflow associated with a series of downbursts on 16 July 1980. Mon. Wea. Rev.,109, 1438-1456.

Johns, R. H. 1993: Meteorological conditions associated with bow echo development in convective storms. Wea. Forecasting, 8, 294-299.

Knupp, K.R., 1989: Numerical simulation of low-level downdraft initiation within precipitating cumulonimbi: Some preliminary results. Mon. Wea. Rev., 117, 1517-1529.

Knupp, K. R., 1996: Structure and evolution of a long-lived, microburst producing storm. Mon.Wea. Rev., 124, 2785–2806.

Laviola, S., Levizzani, V., Ferraro, R. R., and Beauchamp, J., 2020: Hailstorm Detection by Satellite Microwave Radiometers. Remote Sensing, 12(4), 621.

Liu, G., J.A. Curry, and R.W. Sheu, 1995: Classification of clouds over the western equatorial Pacific Ocean using combined infrared and microwave satellite data. Journal of Geophysical Research: Atmospheres, 100(D7), 13811-13826.

Martner, B. E., D.B. Wuertz, B.B. Stankov, R.G. Strauch, E.R. Westwater, K.S. Gage, and W.F. Dabberdt, 1993: An evaluation of wind profiler, RASS, and microwave radiometer performance. Bulletin of the American Meteorological Society, 74(4), 599-614.

Nalli, N.R.; Tan, C.; Warner, J.; Divakarla, M.; Gambacorta, A.; Wilson, M.; Zhu, T.; Wang, T.; Wei, Z.; Pryor, K.; Kalluri, S.; Zhou, L.; Sweeney, C.; Baier, B.C.; McKain, K.; Wunch, D.; Deutscher, N.M.; Hase, F.; Iraci, L.T.; Kivi, R.; Morino, I.; Notholt, J.; Ohyama, H.; Pollard, D.F.; Té, Y.; Velazco, V.A.; Warneke, T.; Sussmann, R.; Rettinger, M. Validation of Carbon Trace Gas Profile Retrievals from the NOAA-Unique Combined Atmospheric Processing System for the Cross-Track Infrared Sounder. Remote Sens. 2020, 12, 3245. https://doi.org/10.3390/rs12193245

Proctor, F.H., 1989: Numerical simulations of an isolated microburst. Part II: Sensitivity experiments. J. Atmos. Sci., 46, 2143-2165.

Pryor, K. L., 2015: Progress and Developments of Downburst Prediction Applications of GOES. Wea. Forecasting, 30, 1182–1200, DOI: 10.1175/WAF-D-14-00106.1.

Pryor, K.L., 2017: Advances in downburst monitoring and prediction with GOES-16. In 17th conf. on mesoscale processes, San Diego, CA, Amer. Meteor. Soc., Paper No. 10.6.

Przybylinski, R.W., 1995: The bow echo. Observations, numerical simulations, and severe weather detection methods. Wea. Forecasting, 10, 203-218.

Schaefer, J. T., 1986: The Dryline. Mesoscale Meteorology and Forecasting, P. S. Ray, Ed., American Meteorological Society, 549-572.

Schroeder, J. L., W. S. Burgett, K. B. Haynie, I. Sonmez, G. D. Skwira, A. L. Doggett, and J. W. Lipe, 2005: The West Texas Mesonet: A technical overview. J. Atmos. Oceanic Technol., 22, 211–222

Smith, B. E., 1990: Mesoscale structure of a derecho-producing convective system: The southern Great Plains storms of May 4 1989. Preprints, 16th Conf on Severe Local Storms, Kananaskis Park, AB, Canada, Amer. Meteor. Soc., 428-433.

Smull, B. F., and R. A. Houze, Jr., 1987: Rear inflow in squall lines with trailing stratiform precipitation. Mon. Wea. Rev., 115, 2869-2889.

Spencer, R.W., H.M. Goodman, and R.E. Hood, 1989: Precipitation retrieval over land and ocean with the SSM/I: Identification and characteristics of the scattering signal. Journal of Atmospheric and Oceanic Technology, 6(2), 254-273.

Srivastava, R.C., 1987: A model of intense downdrafts driven by the melting and evaporation of precipitation. J. Atmos. Sci., 44, 1752-1773.

Wakimoto, R. M., 1985: Forecasting dry microburst activity over the high plains. Mon. Wea. Rev., 113, 1131–1143.

Weisman, M. L., J.B. Klemp, and R. Rotunno, 1988: Structure and evolution of numerically simulated squall lines. J. Atmos. Sci., 45, 1990-2013.

Weisman, M. L., 1992: The role of convectively generated rear inflow jets in the evolution of long-lived mesoconvective systems. J. Atmos. Sci., 49, 1826–1847.

Westwater, E. R., S. Crewell, and C. Matzler, 2005: Surface-based microwave and millimeter wave radiometric remote sensing of the troposphere: A tutorial. IEEE Geoscience and Remote Sensing Society Newsletter, 134, 16-33.

Ziegler, C. L., T. J. Lee, and R. A. Pielke, 1997: Convective Initiation at the Dryline: A Modeling Study. Monthly Weather Review, 125, 1001-1026.

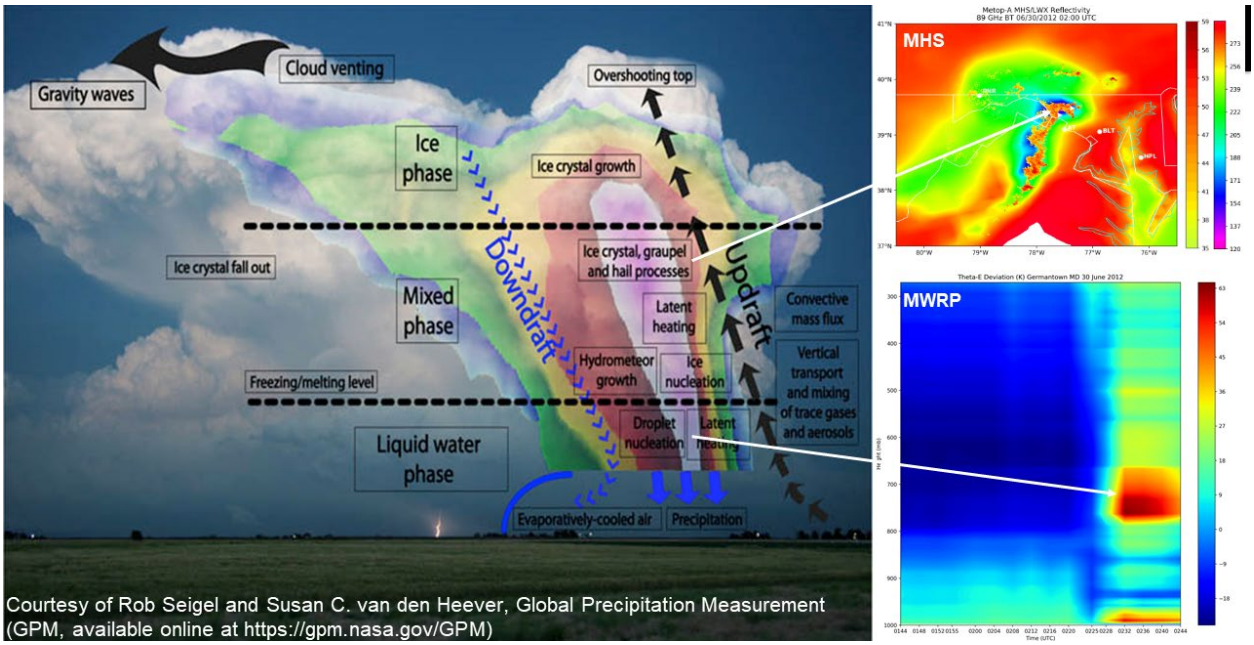

Figure 1. (a) Conceptual model of a deep convective storm; (b-c) microwave imagery examples from satellite- and ground-based sensors, respectively, that demonstrate an improvement in the inference of storm structural characteristics.

METOP-A Infrared Atmospheric Sounding Interferometer (IASI)	METOP-A Microwave Humidity Sounder (MHS)	Ground-based Microwave Radiometer Profiler (MWRP)
• Thermal infrared interferometer measuring 8461 spectral samples between 3.62 and 15.5 um. • Vertical temperature and water-vapor profiles on a 90-level grid extending between 0.005 and 1050 hPa. • Level 2 IASI Product Processing Facility (PPF) version 5:	• High-frequency profiler: 5 channels between 89 – 190 GHz. • Measures cloud liquid water content. • High spatial resolution: 16.7 km at nadir. • Ingested into IASI for the cloud detection process:	• Radiometrics Corporation MP-3000 series units sited at Germantown and Beltsville, MD. • Brightness temperatures in 12 frequency bands from 22 to 59 GHz. • Temperature and humidity soundings up to 10 km height. • Validate IASI T/q profiles.

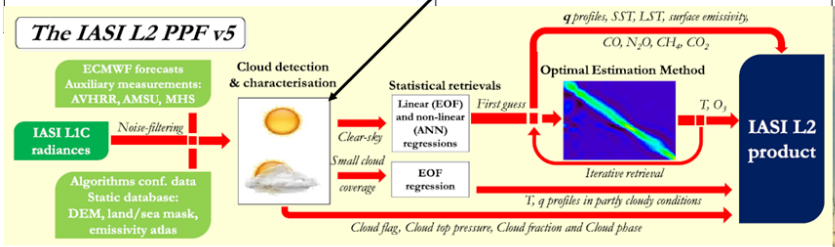

Fig. 1. Modular representation of the IASI Level 2 operational processing chain (version 5), operational since 14/09/2010.

Courtesy August et al. (2012)

Figure 2. A summary of observational remote sensing data applied for the study and analysis of the June 2012 North American Derecho.

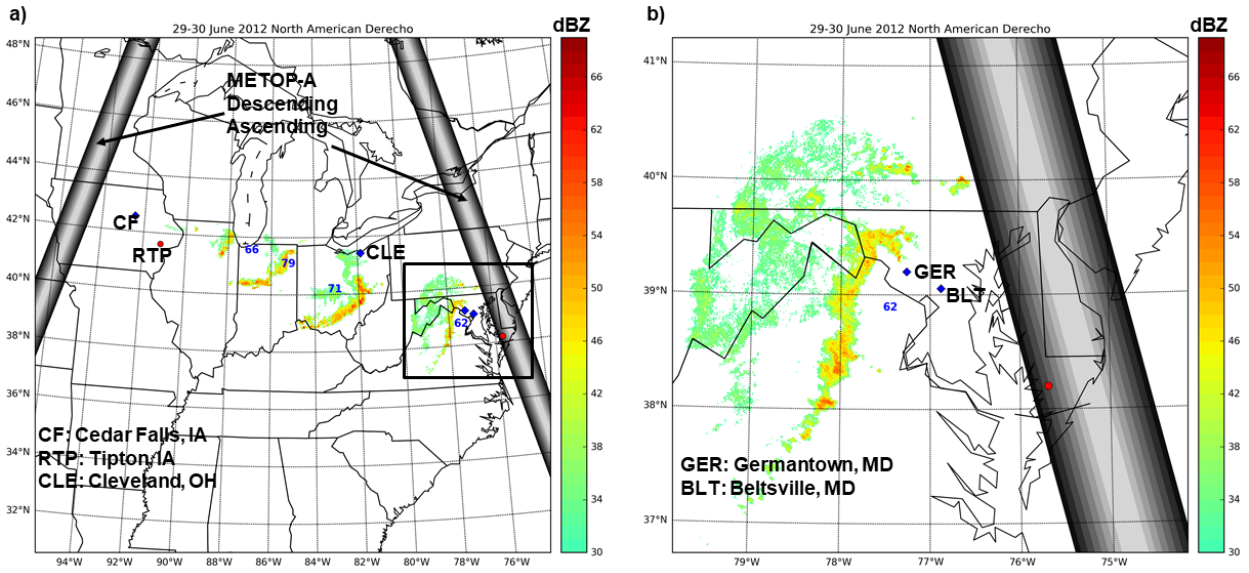

Figure 3. Summary composite image of the June 2012 North American Derecho displaying the 29 June descending node and 30 June ascending node METOP-A orbit tracks, radar reflectivity (dBZ), and significant wind reports (kt) over a) eastern CONUS and b) the Mid-Atlantic region along the storm track. Red circle in b) marks the IASI retrieval location near Salisbury, Maryland.

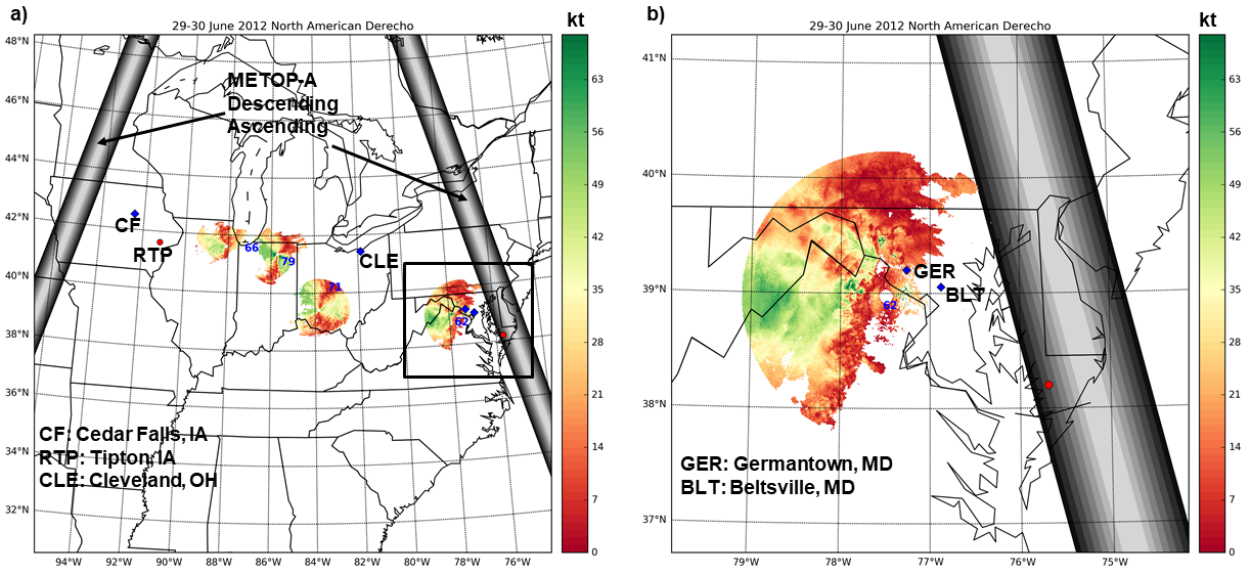

Figure 4. Summary composite image of the 29-30 June 2012 North American Derecho displaying the 29 June descending node and 30 June ascending node METOP-A orbit tracks, NEXRAD radial velocity (kt), and significant wind reports (kt) over a) eastern CONUS and b) the Mid-Atlantic region along the storm track. Red circle in b) marks the IASI retrieval location near Salisbury, Maryland.

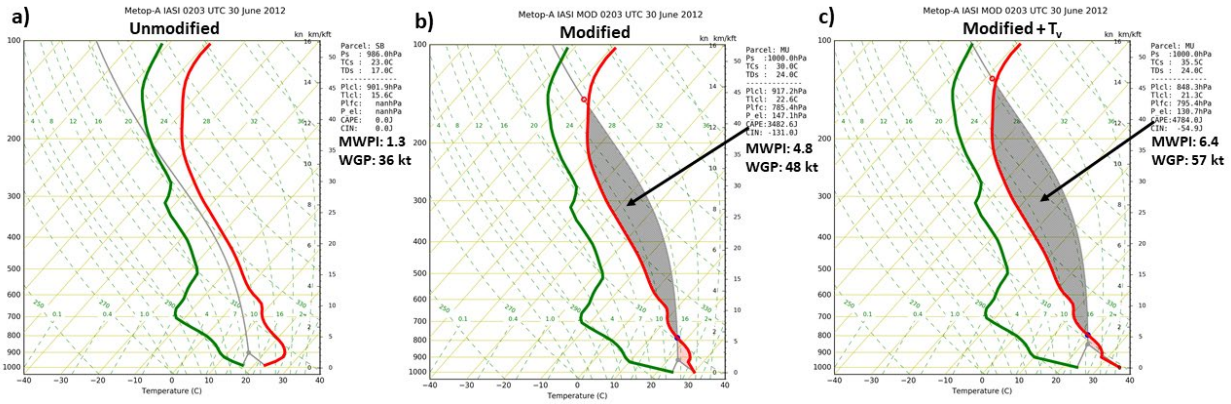

Figure 5. METOP-A IASI retrievals near Salisbury, Maryland during the evening of 29 June 2012 (0203 UTC 30 June): (a) IR+MW sounding profile; (b) IR+MW sounding profile modified by observed surface temperature and dew point at Salisbury Regional Airport; (c) modified IR+MW sounding profile plotted with virtual temperature.

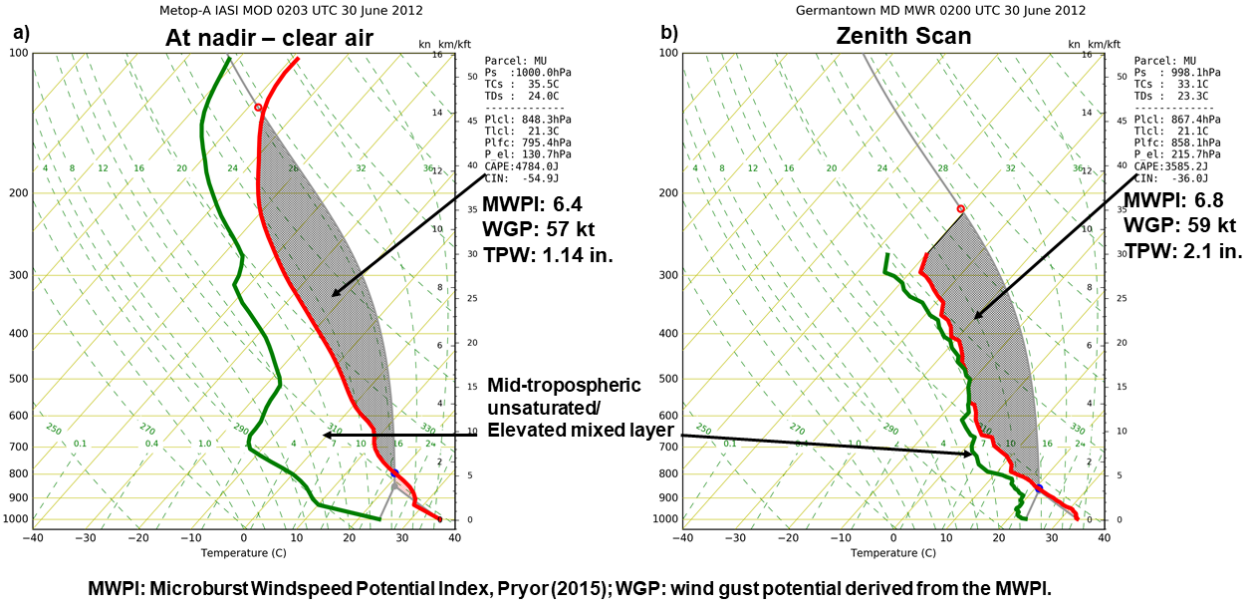

MWPI: Microburst Windspeed Potential Index, Pryor (2015); WGP: wind gust potential derived from the MWPI.

Figure 6. (a) Modified METOP-A IASI IR+MW sounding profile retrieved near Salisbury, Maryland at 0203 UTC 30 June 2012 as compared to (b) a ground-based sounding profile retrieval from the Germantown, Maryland microwave radiometer (MWR).

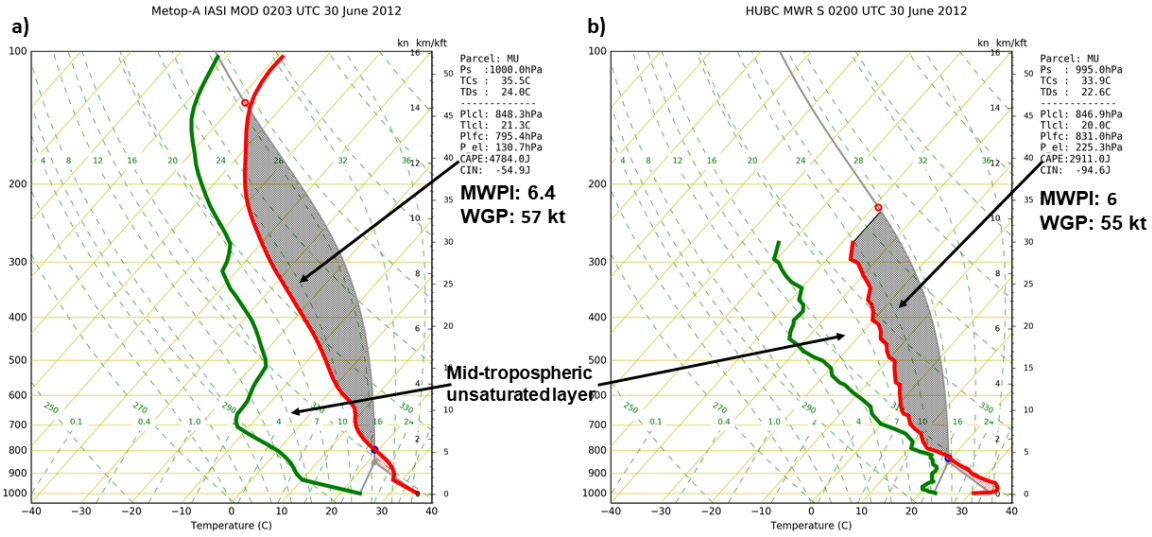

Figure 7. (a) Modified METOP-A IASI IR+MW sounding profile retrieved near Salisbury, Maryland at 0203 UTC 30 June 2012 as compared to (b) a ground-based sounding profile retrieval from the Howard University, Beltsville, Maryland (HUBC) microwave radiometer (MWR).

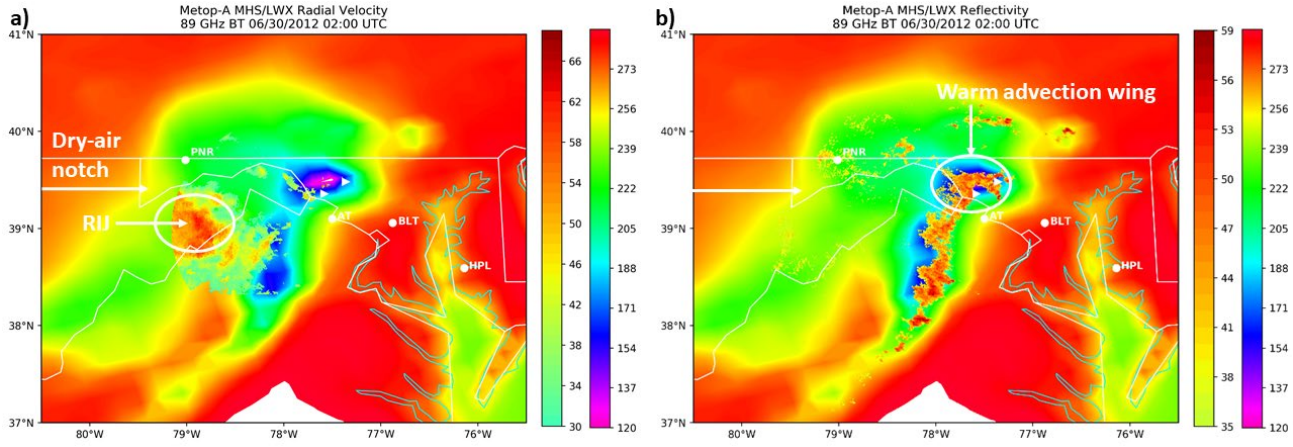

Figure 8. METOP-A MHS 89 GHz brightness temperature (TB, K) image at 0200 UTC 30 June 2012 with (a) overlying Sterling, Virginia (LWX) NEXRAD radial velocity (kt) and (b) reflectivity (dBZ) measurements.

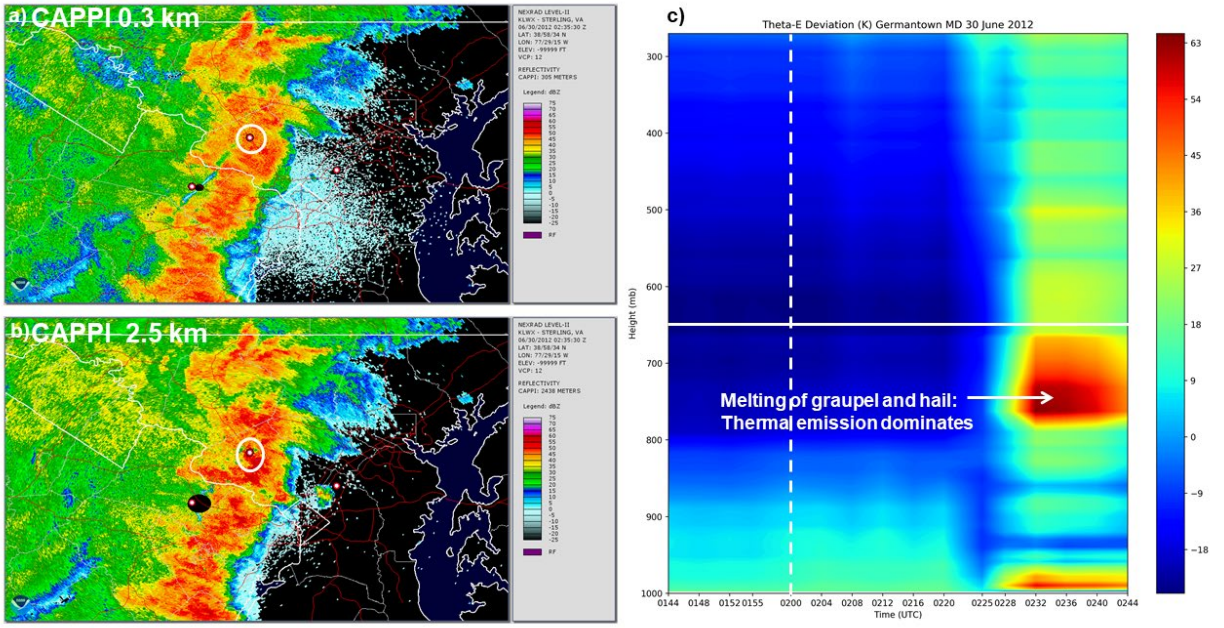

Figure 9. a) – b) Sterling, Virginia NEXRAD Constant Altitude – Plan Position Indicator (CAPPI) reflectivity (dBZ) at 0.3 and 2.5 km altitude, respectively at 0235 UTC 30 June 2012; c) 0144 to 0244 UTC 30 June 2012 time-height cross-section of the deviation of equivalent potential temperature (K) as derived from Germantown, Maryland MWRP.

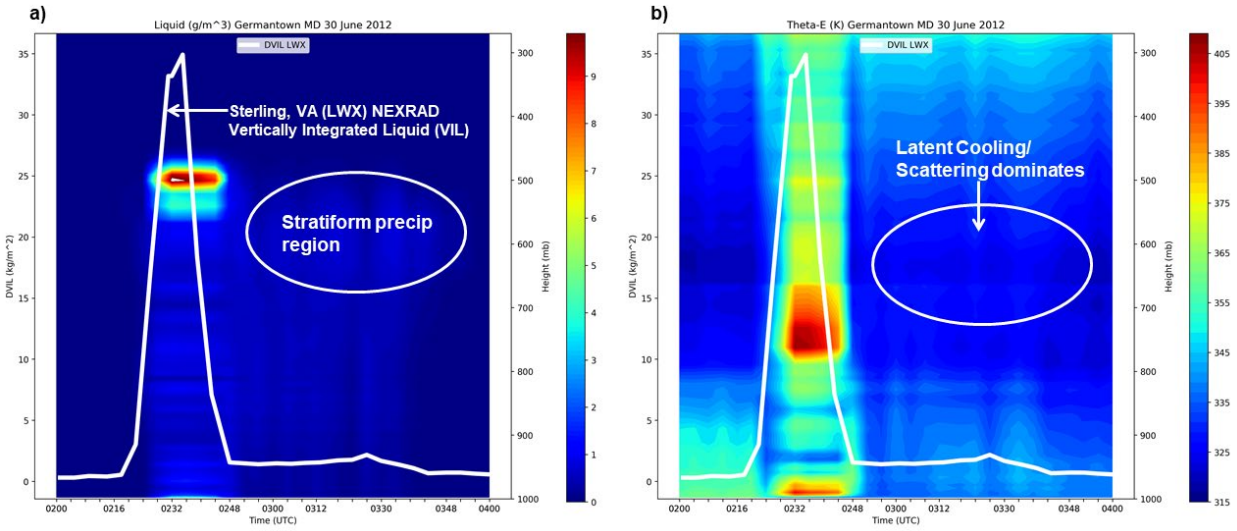

Figure 10. 0200 to 0400 UTC 30 June 2012 time-height cross-sections of a) liquid density (g m^{-3}) and b) equivalent potential temperature (θ_e) as derived from Germantown, Maryland MWRP. Sterling, Virginia NEXRAD DVIL is plotted over the cross-sections at corresponding MWRP retrieval times.

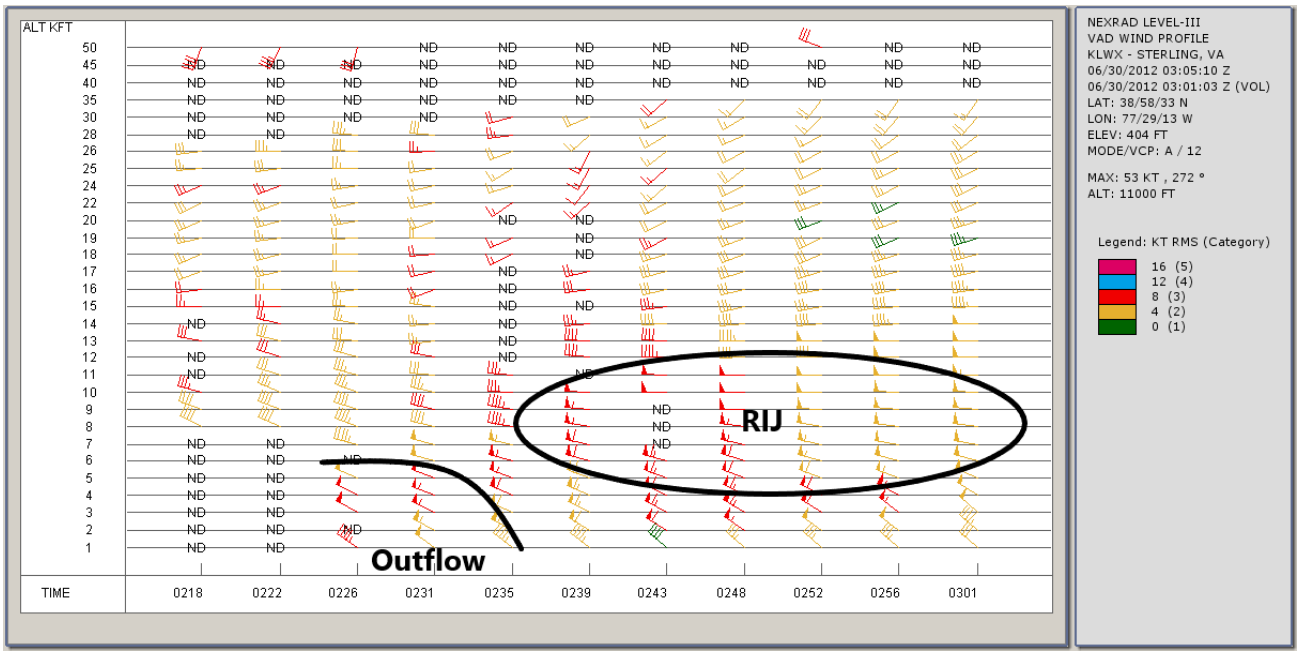

Figure 11. Velocity azimuth display (VAD) wind profile (VWP) from Sterling, Virginia NEXRAD between 0200 and 0300 UTC 30 June 2012.

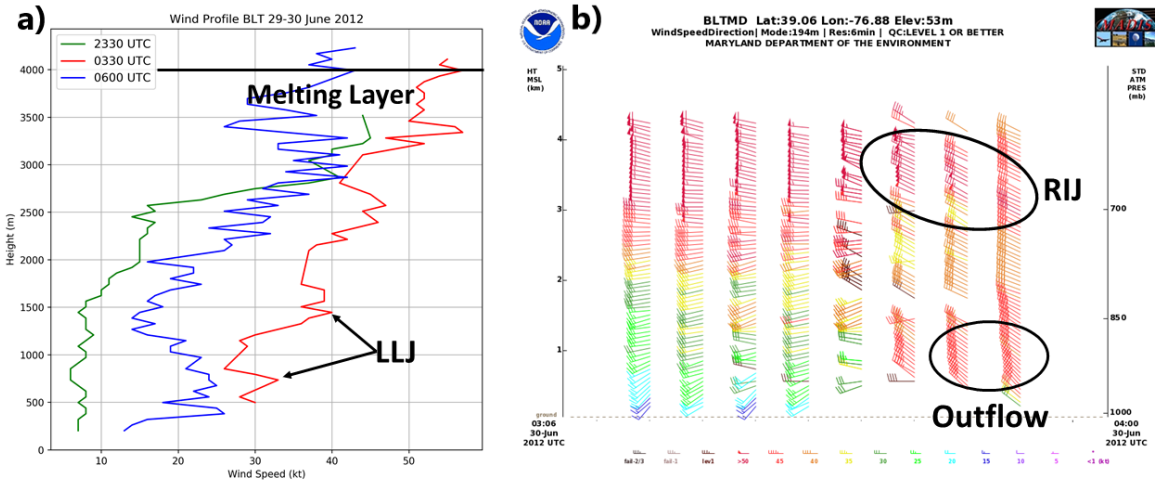

Figure 12. Time series of HUBC 915 MHz Boundary Layer Profiler (BLP) a) wind speed vs height (meters) between 2330 UTC 29 June and 0600 UTC 30 June 2012 and b) wind speed and direction vs height between 0300 and 0400 UTC 30 June 2012.